Fine Structure of a Periciliary Ridge Complex of Frog Retinal Rod Cells Revealed by Ultrahigh Resolution Scanning Electron Microscopy

KLAUS-RUEDIGER PETERS*, GEORGE E. PALADE*, BARBARA G. SCHNEIDER, and DAVID S. PAPERMASTER

** Section of Cell Biology, Yale University School of Medicine, New Haven, Connecticut 06510; and Department of Pathology, Yale University School of Medicine and Veterans Administration Medical Center, West Haven, Connecticut 06516*

ABSTRACT We studied the junctional region between rod inner segments (RIS) and outer segments (ROS) in frog retinas by high resolution scanning electron microscopy (SEM). Retinas of dark adapted or light exposed *Rana pipiens* were critical-point-dried and RIS and ROS were split and coated with ultrathin metal films of niobium and chromium—or decorated with gold—and imaged in a new SE-I imaging mode. The connecting cilium (CC) usually broke at the base of the RIS and remained attached to the ROS. The outer part of the CC plasmalemma expanded to form liplike protrusions beyond which disks evaginated with successively larger diameter until they reached the full width of the ROS. The CC rose out from an invagination of the RIS apical plasma membrane (PM). On the lateral walls of this invagination, a highly ordered complex of nine symmetrically arrayed ridges and grooves rose steeply and extended laterally ~0.4–1 μm on the adjacent RIS PM. On the apical plasmalemma, the ridges and grooves formed groups of three to four parallel rows that surrounded the invagination. The grooves were bridged by filaments anchored at the top edges of the ridges. This highly ordered structure we term the periciliary ridge complex (PRC). Its ninefold symmetry apparently reflects the 9+0 microtubule organization of the CC axoneme. The three-dimensional structure revealed by SEM was confirmed by transmission electron microscopy (TEM) of sections of Epon-embedded retinas. TEM-immunocytochemistry on thin sections of retinas embedded in glutaraldehyde cross-linked albumin suggested that the PRC and the CC may participate in opsin transport and disk morphogenesis.

Polarized cells are able to synthesize and distribute their plasmalemmal molecules to sites of function that often reside on only one domain of their surface. To achieve polarization, such cells must vectorially transport newly synthesized membrane proteins and assemble them into distinct, functionally differentiated plasmalemmal domains; moreover, they must stabilize these assemblies against intermixing with the components of adjacent areas of the plasmalemma and they must ensure a selective turnover of the molecules of each domain.

The photoreceptor cells of vertebrate retinas, the retinal rod, and cone cells are polarized to a remarkable degree; they have separated some of the steps involved in membrane biosynthesis, assembly, and turnover into different cell segments (30, 44). These elongated cells have a unique, complex, light sensitive outer segment (OS) at one end, separated from the adjacent inner segment (IS) by a deep constriction. The gap between the two segments is bridged only by a connecting cilium (CC). The relative isolation of the two segments facilitates the investigation of the successive steps involved in polarized membrane biosynthesis. The IS of retinal rods contains the cell's endoplasmic reticulum and Golgi complex which are located near the nucleus. Between this region and the root of the CC nearly all of the cell's mitochondria are tightly clustered. The rod outer segment contains a stack of photosensitive, rhodopsin-laden disks. The plasma membrane covers the outer segment, the connecting cilium, the inner segment, and the synaptic processes as a continuous envelope, and appears to have differentiated domains on each of these cell parts.

THE JOURNAL OF CELL BIOLOGY · VOLUME 96 JANUARY 1983 265–276

The disk membranes of the outer segment undergo continuous renewal in adult life (45, 46) at a rate that appears to be without equal among other cell types. In the toad *Xenopus laevis*, for instance, about 80 disks of ~7 μm in diameter are generated every day, each disk containing ~1 × 10^6 molecules of rhodopsin (3, 12). Yet the OS lacks the equipment needed for protein synthesis and receives its disk membrane proteins from the IS.

The connecting cilium is the obvious candidate for the pathway in the transport of opsin from its site of synthesis in the IS to its site of function in the OS. By autoradiography, Young (44) observed the clustering of newly synthesized proteins close to the root of the connecting cilium, before they appeared in proximal OS disks. Basinger et al. (2) showed that newly inserted radio-labeled proteins diffused throughout the plasma membrane of the ROS. Papermaster et al. (23, 24) showed that both newly synthesized opsin and a large intrinsic disk membrane protein were associated with readily sedimentable membranes from the earliest stages in their synthesis until they emerged in the OS where they are assembled into a disk and its margins and incisures, respectively (26, 31). Kinney and Fischer (15) observed vesicles close to the proximal end of the CC. Besharse and Pfenninger (4) found that the vesicle membranes had intramembranous particles comparable in size to those seen in the CC plasmalemma and OS disks, but different from those found in the IS plasmalemma except near the cilium. Despite the absence of a transient *N*-terminal signal sequence in the opsin mRNA translation product (28, 40), in vitro translation of opsin mRNA in the presence of dog pancreas microsomes resulted in co-translational insertion of opsin into microsomal membranes (10). Finally, immunocytochemical localization of opsin with antiopsin antibodies applied to thin sections of albumin embedded retinas revealed labeling of RER, Golgi complex, and the vesicles both beneath the CC and in the plasma membrane covering the CC (25, 27, 30).

Together these results support the hypothesis that rhodopsin is an intrinsic membrane protein during all stages of its biosynthesis, posttranslational modifications, and vectorial transport to the OS. Opsin may be inserted (via vesicle fusion) in the apical membrane of the IS and may reach the OS by moving along the plasmalemma of the CC. These last stages of fusion and transport on the CC plasmalemma remain to be established by appropriate procedures.

Because the exact pathway from IS to OS is still uncertain, we carried out a study of the connecting cilium and adjacent structures using recently developed improvements in high resolution scanning electron microscopy (SEM) (34, 35). With these improved techniques, we detected a new structural complex surrounding the base of the connecting cilium in frog photoreceptors (36) which we have termed the periciliary ridge complex (PRC). Parts of this complex were previously seen in replicas of freeze-fractured specimens of lower vertebrates by Andrews (1). But the full visualization of the complex in three dimensions became possible only by high resolution SEM. The PRC may function as a collecting device for opsin before its transport to the OS via the plasma membrane of the connecting cilium.

MATERIALS AND METHODS

Tissue preparation for SEM: Retinas, isolated either under dim red light from frogs (*Rana pipiens*) dark adapted for 16 h, or under room light after 30 min of exposure, were submerged in frog heart Ringer's (FR) (9), adjusted with glucose to 280 mOsmol. The pigment epithelium (PE) was gently but incompletely removed and PE-free areas were collected, washed for 5 min in small test tubes under oscillating movement in fresh FR, fixed in glutaraldehyde (2% [vol/vol] in FR) for 45 min, washed twice with FR (10 min each), postfixed for 2 h in 1% OsO_4 in FR, washed twice with FR (10 min each), and transferred into BEEM capsule (Better Equipment for Electron Microscopy Inc., Bronx, NY) containers for dehydration and critical-point-drying according to the exchange method described in detail earlier (32). After critical-point-drying in CO_2, the tissue was cut into 2-×-2-mm pieces. The photoreceptor surface of the specimens was pressed lightly against 3-×-3-mm squares of double stick SCOTCH tape (3M Corp., St. Paul, MN) attached onto silicon wafer chips (Monsanto Co., Dedham, MA). The tissue was carefully peeled off the tape and mounted (next to the tape) on the chip with DAG 154 carbon paint (Acheson Colloids Co., Port Huron, MI), the newly exposed surface pointing upward. This step resulted in the fracture of most connecting cilia and the extensive separation of the layer of IS (which remained within the tissue block) from the layer of OS (which was peeled away) (see Fig. 1). Extensive specimen volume loss is known to occur during this preparation procedure (6). In our specimens, IS shrank more than OS, but the periciliary invagination was not markedly affected in SEM of dried specimens. Its general dimensions (depth and width) were similar to those viewed in unfixed living cells by video-enhanced high resolution interference-contrast light microscopy (29).

Metal Coating of SEM Samples: The specimens were coated by Penning sputtering (14), a newly introduced metal coating method which was found superior to all other coating techniques tested (33) because it could generate metal films <2.0 nm in average mass thickness, deposited at reduced crystal size and increased film continuity. The Penning sputter-coater (PSC model 1a) was obtained from the Zentrum für Elekronenmikroskopie (Graz, Austria). A detailed description of the metalization procedure is given in Peters (33). For general survey micrographs, we used thin- (3–5 nm) gold-coating, whereas for fine structural observations we relied on Nb and Cr films (1 to 2 nm). The thickness of the metal films was measured with the highest accuracy now possible using a XTM quartz monitor from Inficon Leybold-Heraeus Inc. (East Syracuse, NY) during metal deposition which was carried out in a modified Balzers vacuum evaporation unit (BEA 120: Balzers High Vacuum Corp., Nashua, NH) with the specimen under continuous tumbling motion provided by a Samspin device (Tousimis Research Corp., Rockville, MD). The metal thickness was measured as average mass thickness with an accuracy better than 20 pm/20 $g \cdot cm^{-3}$. The values refer to the normal direction on surface areas fully exposed to the metal source during coating.

High Resolution SE-I SEM: For high resolution SEM, we selectively used secondary electrons (SE) generated on the specimen surface by the electron probe in its spot of incidence (SE-I image mode [34]). The production of other secondary electrons, at some distance from the probe site, by backscattered electrons (BSE) on the specimen (SE-II) or on the pole piece of the final lens (SE-III) was suppressed or eliminated. The signal collection for SE-I was improved by shielding the specimen from the specimen chamber with a carbon-coated aluminum plate (BSE absorption plate [35]), which eliminates the SE-III component from the total SE signal. Reduction of the SE-II component was achieved by using low atomic number metals, e.g., Nb and Cr, for coating. Such metals give a higher SE-I/SE-II ratio (42) than the conventionally used high atomic number metals (gold and platinum). The SE-II component of the signal was further reduced by applying metal films ~2.0 nm thick, and by operating the scanning microscope at a high acceleration voltage, i.e., 30 keV. In this work a cold field emission microscope (JEOL JFSM 30) was used at 30 keV acceleration voltage and a 13-mm working distance. The instrument was operated with a beam current of $1–3 \cdot 10^{-11}$ A, a beam diameter of ~1 nm at magnifications up to 100,000 times. A JEOL JEM 100 CX, provided with a scanning attachment, was used for monitoring the results of preparation procedures and for preliminary specimen screening.

Transmission Electron Microscope (TEM) Preparation: Retinal tissue (*R. pipiens* and *Rana ridibundi*) was fixed and embedded in epon or in bovine serum albumin (BSA) cross-linked by glutaraldehyde as described previously (16, 18, 25). Thin sections of BSA-embedded retinas were labeled successively with affinity purified rabit anti-frog opsin, biotinyl sheep anti-rabbit $F(ab')_2$, and avidin-ferritin (25). Thin sections cut from BSA or epon embedded blocks were examined in a Philips EM 300 operated at 60 keV.

RESULTS

General Considerations

Each rod or cone photoreceptor cell of the frog retina is divided into an IS and OS segment joined to one another by a short connecting cilium (CC). In specimens critical-point-dried and split as given under Materials and Methods, the connecting cilia of most rod cells usually broke at their bases near the IS, their stumps remaining attached to the correspond-

ing OS (compare Fig. 1, 2, 3, and 5). The fracture of the rod cilia led to full exposure of the apical and basal plasmalemmal domains of the IS and OS, respectively. The surface structure of these domains could be conveniently examined by high resolution SE-I scanning electron microscopy.

Cone cells—generally shorter than rods—split only occasionally, presumably because their tips rarely reached the surface of the adhesive tape used for fracturing the retina. Often only the principal cone OS was detached from the IS of double cones (Fig. 1).

Apical Surface of the Rod Inner Segment

PERICILIARY RIDGE COMPLEX: On all exposed apical plasmalemmal domains of the rod inner segments, SEM revealed the presence of an eccentric conical invagination with indented walls, located near or at the margin of the IS (Fig. 2*a*). The invagination measured ~0.5 μm in diameter and ~0.3 μm in depth and was regularly centered on the site of emergence of the connecting cilium from the IS (Fig. 2*b* and *c*). The wall of the invagination was deeply indented by nine symmetrically arrayed grooves, ~100 nm wide, separated by nine ridges ~80 nm in width that rose steeply from the base (Fig. 2*a* and *b*). As they reached the flat apical surface of the IS, the grooves extended outward 0.4–1.0 μm and formed groups, usually triplets, that diverged from one another and thereby deviated from the initial radial symmetry found in the invagination (Fig. 2*a* and *b*). Along these lateral extensions, the grooves appeared to be shallower than in the invagination proper: a sharp step could be detected between the two parts of the grooves (Figs. 2*b* and 3*a*) when the specimens were tilted at an appropriate angle.

The ridges had the appearance of rigid structures with straight rectangular profiles and relatively sharp edges (Figs. 2 *a* and *b* and 3*a, b, d*). The axis of symmetry of the entire complex was the connecting cilium. This symmetry, already strongly suggested by SEM micrographs (Fig. 2*b*), became clearly evident in TEM of thin sections which were cut perpendicular (or nearly so) to the connecting cilium at the level of the invagination (Fig. 2*c*). Such micrographs showed that each ridge was radially aligned with a longitudinal rib of the ciliary shaft under which one doublet of the nine microtubule doublets of the cilium was located. On the inner surface of the ribs, the ciliary plasmalemma was in contract with a dense, apparently fibrillary infrastructure that connected it with the underlying doublet (Figs. 2*c* and 3*b*). Such micrographs also suggest that delicate fibrillary structures may connect the ciliary ribs to the corresponding ridges of the invagination.

We propose that this newly defined structure, located on the apical surface of the rod inner segment and centered on the point of emergence of the connecting cilium, be called the "periciliary ridge complex."

A similar structural complex is exposed on the apical surface of the inner segment of cone cells (Fig. 2*a*), but the evidence we have at present is not sufficient for a detailed comparative study of this complex in cones with the periciliary ridge complex of rod cells.

Correlation with Structural Information Obtained by TEM

We used the well defined, three-dimensional images of the periciliary ridge complex provided by SEM to assess the information obtained by us and by others by TEM of thin sections through the relevant region of the rod cell. Without precise, recognizable orientation, TEM images are difficult to interpret (in contradistinction to the easily interpretable SEM images). When adequately oriented, TEM micrographs confirm the existence of the invagination (Figs. 2*c and* 3*b*), its eccentric position on the apical surface (Fig. 2*c*), its occasional opening to the lateral surface of IS (Fig. 3*b*), and the presence of well defined ridges and grooves (Figs. 2*c* and 3*b*). TEM micrographs were critical in defining the correlation of the radial symmetry of the complex with that of the cilium and the association of fine fibrillary material with the ridges of the complex and the ribs of the ciliary shaft (Fig. 3*b*). In sections grazing the surface of the ridges, this surface material appeared as fibrillary bands (Fig. 3*b*) of indefinite length and 30–60 nm width. TEM also was valuable for defining the type of structural elements associated with the cytoplasmic aspect of the complex. The ridges themselves appeared to have a fibrillary infrastructure with condensations along their edges; in general they did not contain vesicles or any other type of recognizable subcellular components (Figs. 2*c* and 3*b*). Vesicular profiles were found associated with the grooves especially along the bottom (Fig. 2*c*). Other subcellular components regularly found under the invagination were mitochondria, a basal body, and a centriole.

Fine Topographical Detail of the Periciliary Ridge Complex

The high resolution attained in our SEM micrographs made possible the detection of the following elements of surface fine structure. On ridge surfaces of the apical plasmalemma domains, gold crystal decoration took the form of globular particles 10–20 nm in diameter (Figs. 2*b* and 3*a*) preferentially located along the sharp edges of the ridges. Along these edges the particles formed rows in which they appeared distributed at an average spacing of ~30 nm. Similar particles were seen on the juxtaciliary aspect of the ridges and—at lower surface density—on the sides of the grooves and on the rest of the apical plasmalemma (Figs. 2*b* and 3*a*).

Micrographs of specimens coated with a thin continuous film of low atomic number metals (i.e., Cr and Nb) revealed additional surface details (Fig. 3*c* and *d*). Between edges, opposite to each other on either side of the grooves, filaments were seen bridging the grooves (Fig. 3*c*). The ridge edges were formed by ~30-nm particles to which the filaments were attached in some cases. The filaments themselves appeared irregularly deformed and often broken (Fig. 3*d*).

Main Apical Features of the PRC

The most common structural pattern of the PRC seen on the apical plasmalemma consisted of three groups with three parallel grooves in each group separating and flanking two parallel ridges (Figs. 2*a* and *b* and 3*a* and *c*). The triplets were disposed symmetrically around the invagination and were separated from one another by a ~120° angle, the wedge of this angle corresponding to (or replacing) one or two ridges (Fig. 4). Although the three triplet pattern was the most frequent arrangement of the complex, many variations on this theme were encountered. They affected the number of grooves (and ridges) per group—which could be as low as two or as high as five (Fig. 2*a*)—, the angle separating two groups—which could be as narrow as 30° or as wide as 180° (Fig. 2*a*)—, and the position of the invagination—which was often located so close to the rim of the apical plasmalemma that part of its circular wall was missing and some of its ridges were provided by

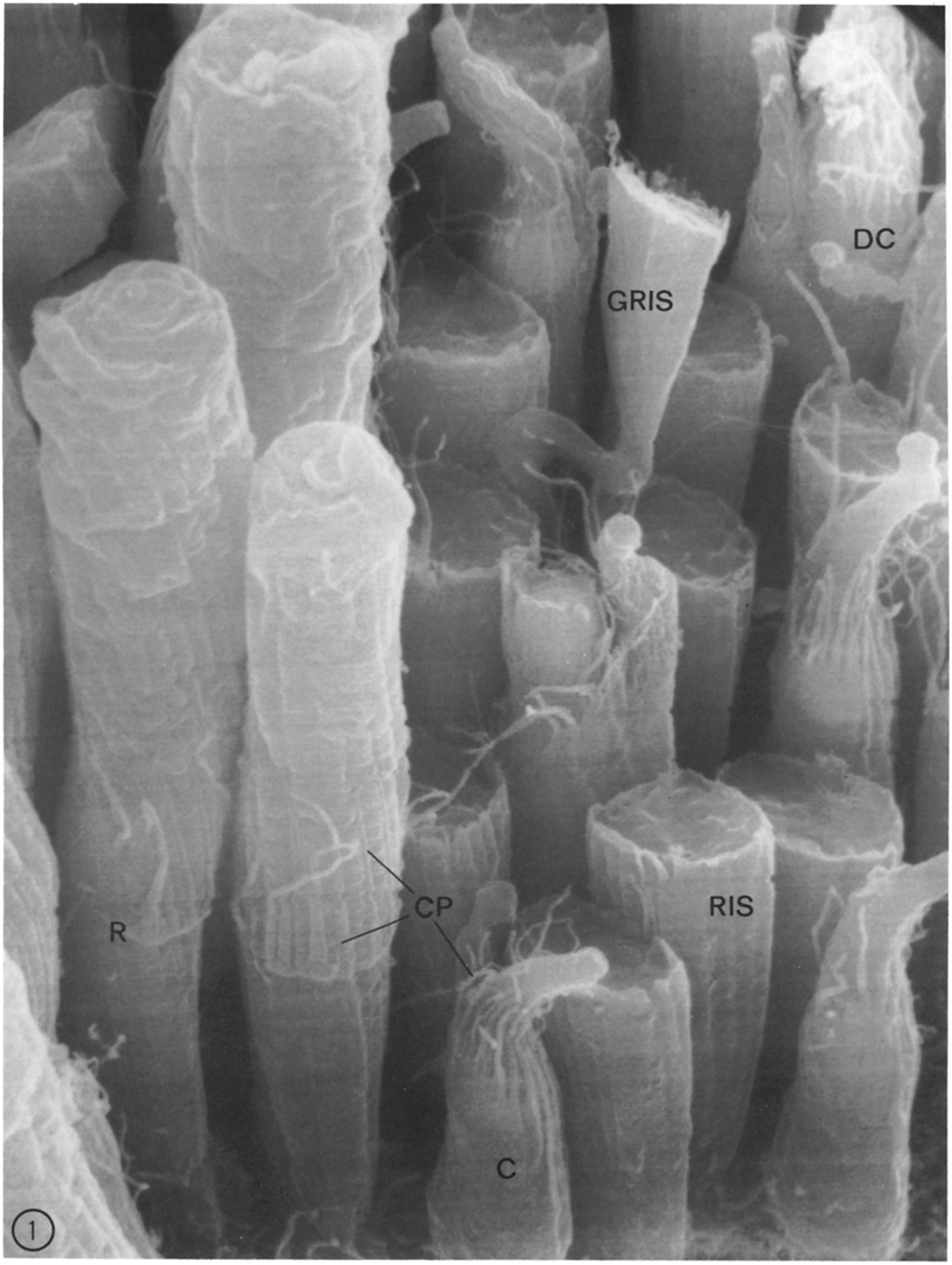

FIGURE 1 Frog retina. Rod photoreceptors were split leaving their inner segments behind after removal of the corresponding outer segments (right). A few intact rods (left) and cones remain. *(C)*, Intact cone cells. *(CP)* Calycal processes. *(DC)* Intact double cone. *(GRIS)* Green rod inner segment. *(R)* Intact rod cells. *(RIS)* Rod inner segments. Gold decorated with 5.0 nm average mass thickness. × 10,000.

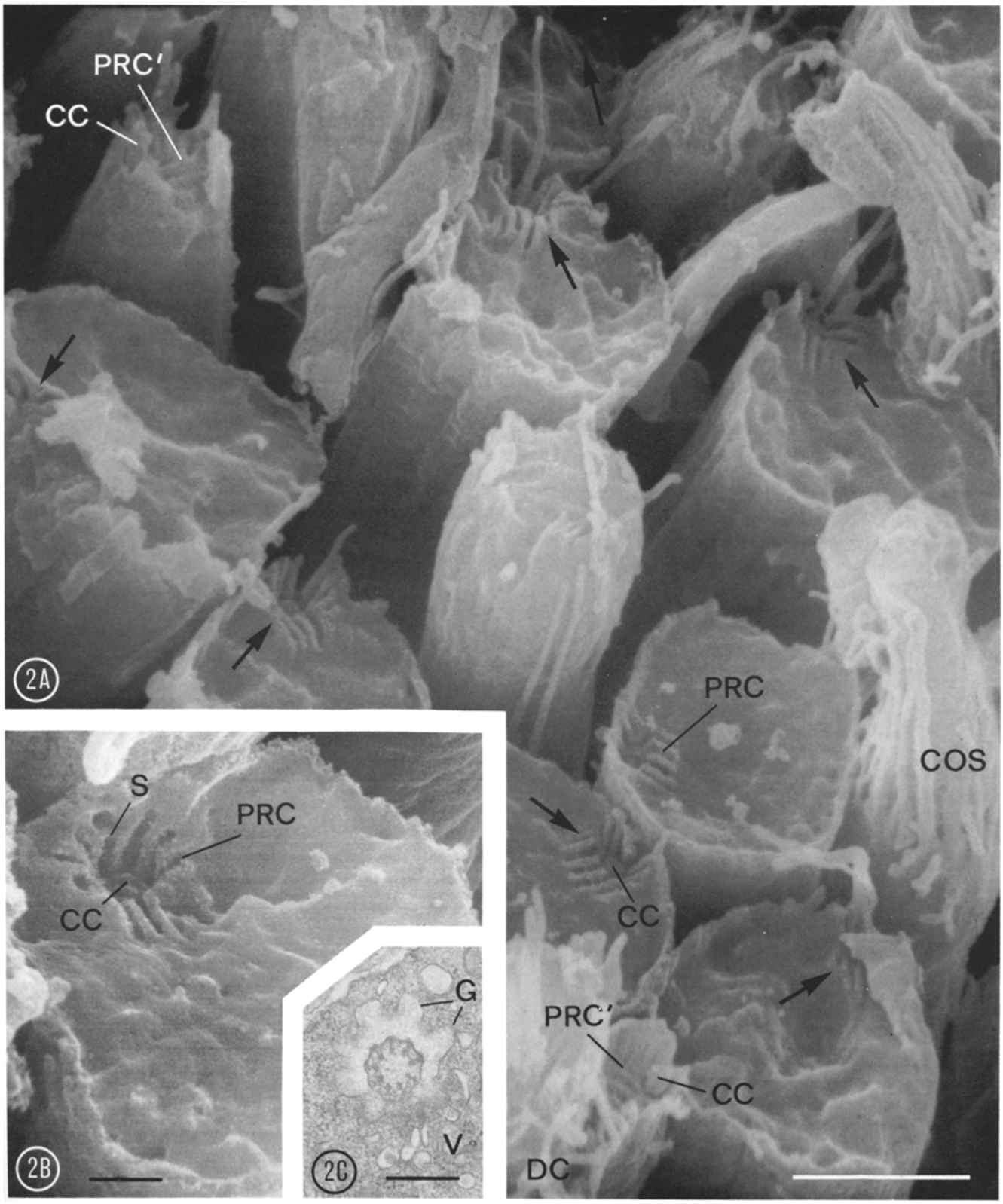

FIGURE 2 *(A)* Exposed apical domains of rod inner segments. Periciliary ridge complex (*PRC*, arrows), each consisting of a deep invagination, surrounds the proximal end of the connecting cilium *(CC)* (fractured during the splitting of the retina). Grooves and rigid ridges are sculpted in the wall of the invagination and extend laterally on the apical surface of the inner rod segment. *(COS)* Cone outer segment. *(PRC')*, Periciliary ridge complex on the apical surface of the inner segment of a cone cell. Gold decorated with 5.0 nm average mass thickness. Bar, 2 μm. × 16,000. *(B)* Oblique view of a PRC. The stump of the connecting cilium *(CC)* is visible in the center of the invagination. Same coating as in *a*. *(S)* Step between deep and shallow part of a PRC groove. Bar, 0.5 μm. × 26,000. *(C)* Cross-sectioned periciliary ridge complex in a thin section from an Epon-embedded retinal specimen. In the upper half of this image, where the section is perpendicular to the cilium, the 1 to 1 correspondence of ridges and ciliary shaft protrusions (ribs) is clearly visible. Microtubule doublets are located under the ciliary ribs. In the lower half of the field this relationship is blurred by the obliquity of the section. Numerous vesicles *(V)* are present in the surrounding cytoplasm associated mostly with the grooves *(G)* of the complex. Bar, 0.5 μm. × 26,000.

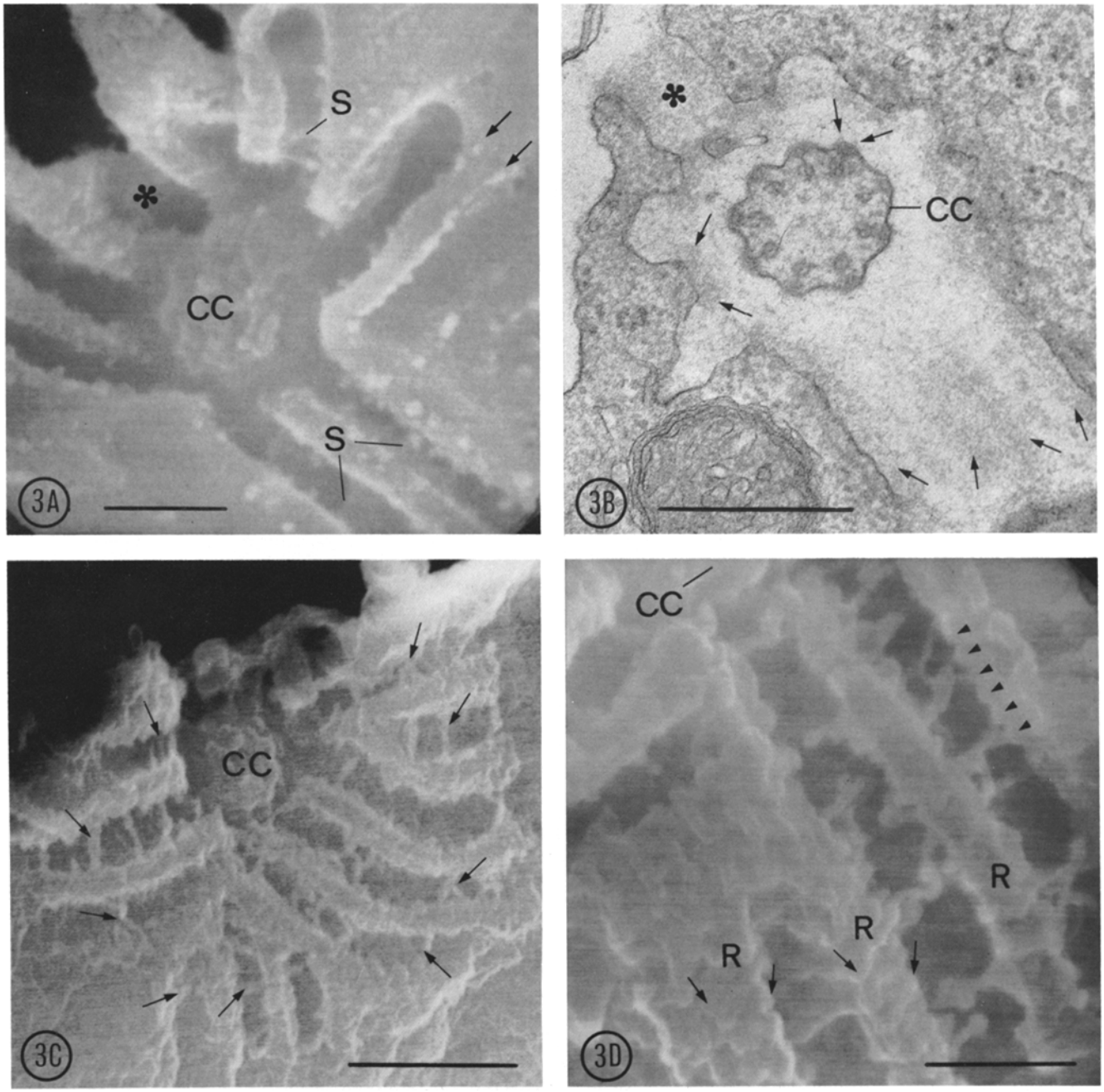

FIGURE 3 *(A)* SEM of a periciliary ridge complex (rod cell), decorated with Au of ~3.0 nm average mass thickness. (*CC*) Stump of the fractured cilium at the bottom of the invagination. (*S*) Step between the deep and shallow part of a PRC groove. Arrows point to decoration by gold crystals that takes the form of rows of particles along the sharp edges of the ridges of the complex. Asterisk indicates groove that extends to the lateral plasmalemma. Bar, 0.2 μm. × 94,000. *(B)* Section cut perpendicularly through the connecting cilium (*CC*) but slightly obliquely through its PRC. The scalloped *CC* profile contains nine peripheral microtubule doublets but no central pair; density, however, is not homogeneous in the *CC* interior. Each doublet is located under a protrusion of the plasmalemma to which it is connected by a dense "spoke." The section cuts through part of the wall of the invagination (upper left half of the image), but passes along the upper surface of ridges (lower right half). Part of the wall of the invagination is missing (asterisk); the gap may represent a groove which extends through to the lateral plasmalemma. Fine fibrillar material (arrows) covers the edges of the PRC ridges and the protrusions of the ciliary shaft. Bar, 0.5 μm. × 62,000. *(C)* SEM of a periciliary ridge complex, coated with a fine crystalline continuous niobium (Nb) film of 2.0 nm average mass thickness. The grooves are bridged by filaments (arrows) spaced along the edges of the ridges. (*CC*) connecting cilium. Bar, 0.5 μm. × 54,000. *(D)* Partial view of a periciliary ridge complex. Specimen similar to the one in *C*, coated with 2.0 nm thick Nb-film. At high magnification the ridges *(R)* are covered by particles arrayed along their edges (arrows) at ~30-nm spacing (arrowheads). Irregularly spaced filaments connect the ridges across the grooves of the complex. Bar, 0.2 μm. × 120,000.

individual calycal processes, as they extended beyond the IS-OS junction along the sides of the OS (Figs. 2*a* and 3*a*). Rarely, some ridges branched either within the invagination or upon reaching the apical plasmalemma and, occasionally, isolated individual ridges or small groups of parallel ridges appeared to be separated by grooves without a continuous con-

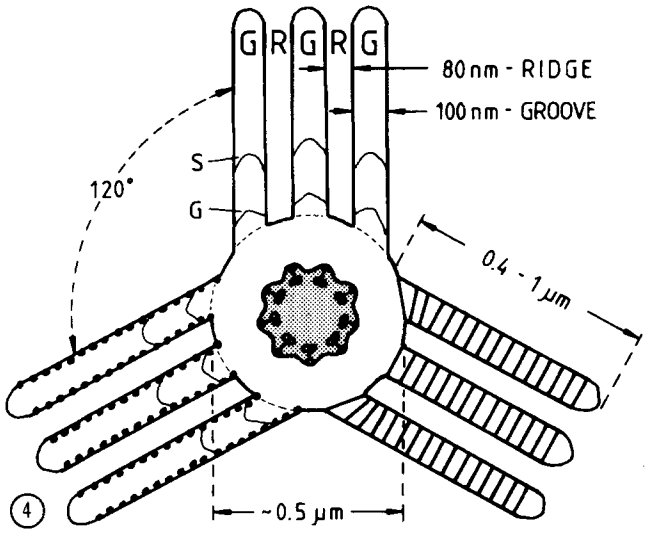

FIGURE 4 Diagram of the main PRC features as seen by SEM on the apical plasmalemmal domain of rod inner segments. The edges of ridges *(R)* are decorated with particles when gold coating was applied (lower left). The grooves *(G)* are spanned span by filaments when niobium coating was used (right). *(G')* Groove in the lateral wall of the invagination. *(S)* Step in groove.

nection with the corresponding structures of the main invagination (Fig. 3 *c*). Common to all PRC was their distinct fine structure. The ridges and grooves of each group were aligned in parallel. The ridges ~80 nm in width were separated by 100-nm-wide grooves and seemed to be anchored to each other by filaments attached to their edges.

Basal Plasmalemmal Domain of the Rod Outer Segment and Connecting Cilium

The periphery of the OS was regularly covered by long (≤ ~5 µm), slender, tapering calycal processes that ran parallel to one another on the outer surface of the OS usually in a groove associated with underlying disk incisures (Fig. 5 *a*). The processes originated from the IS at the level of the OS-IS junction (Figs. 1 and 6 *b*).

The broken connecting cilium was easily recognized because of its eccentric location (Fig. 5 *a*) and characteristic morphology: it had the form of a truncated cone (length: ~0.3–0.4 µm, large diameter: ~0.7 µm; small diameter: ~0.3 µm) or column capital whose surface was provided with longitudinal ribs separated by grooves, arranged with ninefold symmetry (Fig. 5 *b* and *c*). The ribs overlaid the microtubular doublets at the periphery of the cilium (Figs. 2 *c* and 3 *b*). The surface of the cilium was extensively folded, possibly because of local excess of membrane caused by volume loss without parallel surface loss during specimen preparation. The extended folding of the plasma membrane covering the connecting cilium should be contrasted with the taut plasmalemma that covers the ridges of the periciliary complex. The expanding end of the connecting cilium generated lateral protrusions (lips) before expanding into retinal disks of progressively larger dimensions (Fig. 5 *a* and *b*).

The lips showed considerable variation in their topography. In retinas of dark-adapted animals (Fig. 5 *a*), they protruded only a small distance, and only one or two disks, each less than the full ROS diameter in size, were seen expanding above lips from the CC on the basal surface of the ROS. After light exposure, the lips altered their shape. Elongation projections arose in alignment with the ciliary ribs and developed broad bases (Fig. 5 *b*). Several disks emerged above the lips beneath the ROS.

On specimens coated with a fine crystalline Cr film, the ciliary plasmalemma showed, in addition to ~20 nm particles, numerous thin membrane folds, or fine fibrillar structures 1.0–2.0 nm in width disposed perpendicularly to the cilium long axis (Fig. 5 *c*).

Localization of Opsin by Immunocytochemistry

Opsin distribution within the junctional area of the retinal rods was studied on thin sections of fixed specimens embedded in BSA and reacted in succession with rabbit anti-frog opsin, biotinyl sheep anti-rabbit IgG, and avidin-ferritin conjugates, as given under Materials and Methods. High labeling density, i.e., 1,000–2,000 particles/μm^2 section surface, was seen on the stacked disks of the outer segments (Fig. 6 *a*). Dense-labeling was also detected on the plasmalemma of the outer segment and on ciliary lips. These areas were sharply demarcated from the ciliary plasmalemma and from the IS plasmalemma (including its apical domain) that were lightly and discontinuously marked by ferritin complexes. Intracellular vesicles located within the inner segment on both sides of the basal body (and beneath the centriole) were heavily labeled, however. Ferritin clusters scattered at low density were also detected between the profiles of tightly packed mitochondria that filled the remaining cytoplasmic space of the apical portion of the inner segment. Epon sections demonstrated the presence of numerous vesicles (perhaps cisternae) interdigitated between mitochondria and closely packed beneath the invagination (Fig. 6 *b*). We assume that these were the structures labeled by antiopsin in BSA-embedded specimens.

DISCUSSION

A number of improvements in specimen preparation and microscopy (described in detail by Peters in references 32, 33, 34) provided the high resolution and high depth of focus needed for the visualization of the periciliary ridge complex. The thick (10–20 nm) gold coatings conventionally used to amplify the generation of SE on biological specimens, obscure (by blanketing) fine topographical details and generate excessive amounts of BSE and heat under the impact of the primary electron probe, by promoting inelastic electron scattering. BSE emerge at relatively great distances (up to 10 µm) from the site of impact of the electron beam and reduce resolution because they generate in turn additional SE that, under usual operation conditions, are collected in the total SE signal used to produce the image. BSE generate SE from the specimen itself (SE-II), especially when the latter is coated with metals of high atomic number, as well as from the pole piece of the objective (SE-III). When SE-II plus SE-III account for a large fraction of the total SE signal, the high resolution signal generated by the electron probe at the site of impact on the specimen (SE-I) is largely or completely obscured. A BSE signal collected in phase with the SE signal and subtracted from it, produces a more favorable ratio of SE-I to SE-(II+III) and increases surface contrast at low magnification (8) but does not increase resolution at high magnifications (34). We have circumvented these problems by using a new SE-I image mode that achieves a relative enrichment of SE-I in the total SE signal by instrumental modifications (35) and ensures the visualization of

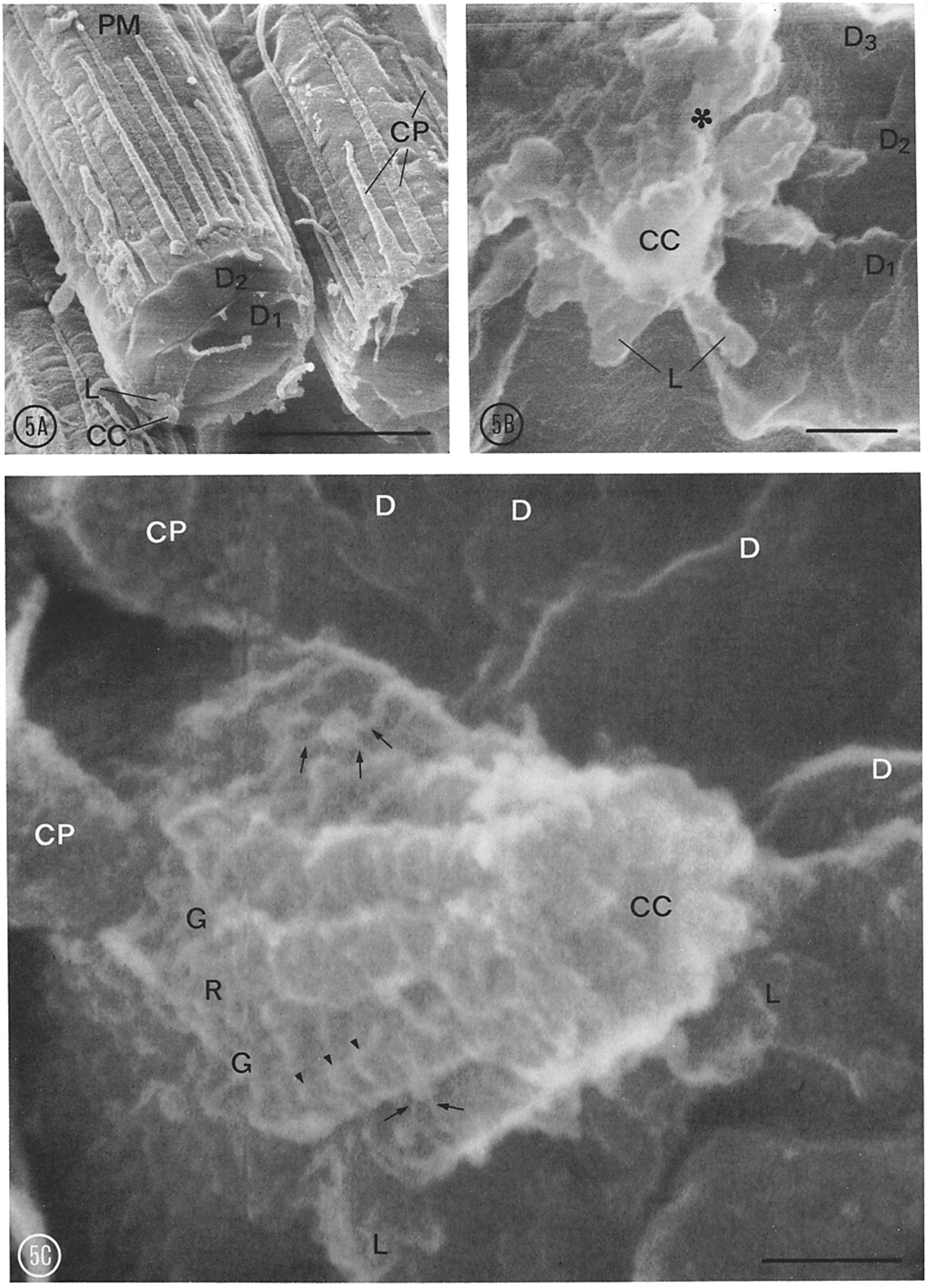
PM
CP
D2
D1
L
CC
5A
D3
*
D2
CC
D1
L
5B
CP
D
D
D
D
CP
G
CC
R
L
G
L
5C

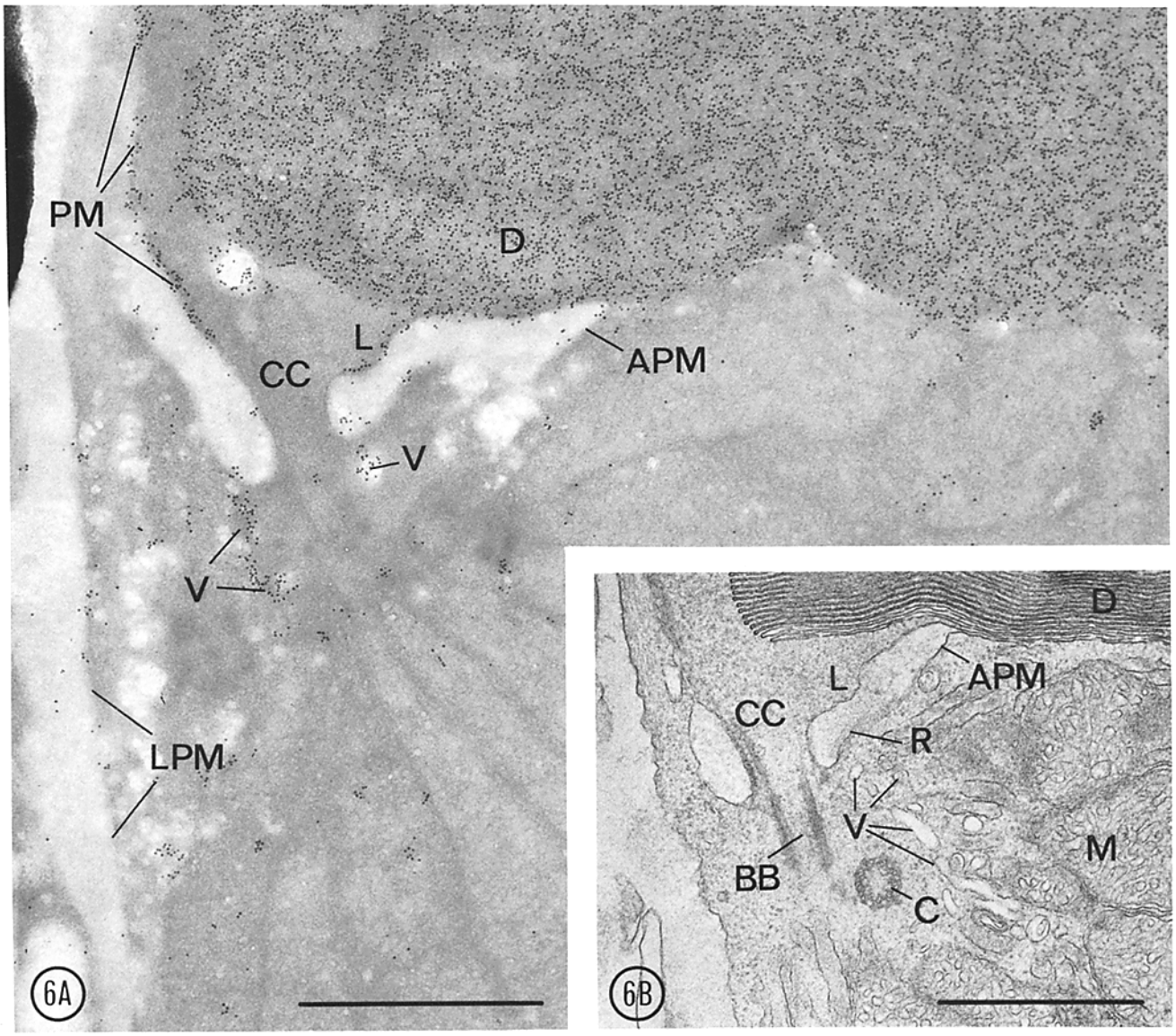

FIGURE 6 *(A)* Immunocytochemical localization of opsin in rod cells. A thin section of albumin embedded frog retina *(R. ridibundi)* was labeled by antiopsin, biotinyl anti-IgG, and avidin-ferritin. Vesicles *(V)* beneath the PRC, the protruding lip *(L)*, and the disk membranes *(D)* of the ROS and its plasmalemma *(PM)* are all densely labeled. The plasma membranes of the lower portion of the connecting cilium *(CC)*, the apical PM *(APM)*, and lateral membrane of the RIS *(LPM)* are either unlabeled, or labeled to a low level above background. Bar, 1 μm. × 36,000. *(B)* Longitudinal section of rod cell: section of frog rod *(R. pipiens)* cuts along the axis of the connecting cilium and reveals structural details in the periciliary ridge complex. *(APM)* Apical plasmalemma of the inner segment. *(BB)* Basal bodies. *(C)* Centriole. *(CC)* Connecting cilium. *(D)* Disks in the outer segment. *(L)* Lip. *(M)* Mitochondria. *(R)* Ridge. *(V)* Carrier vesicles. Bar, 1 μm. × 30,000.

FIGURE 5 *(A)* Rod outer segments. At the basal surface of ROS split from the IS, disks of increasing diameter expand from the outer cilium. *(CC)* Stump of the fractured connecting cilium. *(CP)* Calycal processes along the lower surface of the outer segment. *(D_1* and *D_2)* Disks of progressively larger diameter. *(L)* Protruding lip of the ciliary plasmalemma. *(PM)* Plasmalemma of the outer segment (lateral domain). Gold decorated with 3.0 nm average mass thickness. Bar, 5 μm. × 6,500. *(B)* Basal surface of a rod outer segment from a retina prepared from frogs which spent ½ h in the light part of a 12-h light cycle. Partial view of lip protrusions. Specimen coated with a fine crystalline Nb film of 2.0-nm thickness. *(CC)* Stump of the fractured connecting cilium. *(D_1, D_2,* and *D_3)* Stacked disks still in continuity with the ciliary plasmalemma. *(L)* Lip protrusions. Asterisk indicates lip protrusion expanding at the end of a ciliary rib. Bar, 0.2 μm. × 84,000. *(C)* Connecting cilium. Details of surface fine structure. Specimen coated with a fine crystalline Cr film of 1 nm average mass thickness. *(CC)* Fractured end of the cilium. *(CP)* Fractured calycal process. *(D)* Disk. *(G)* Longitudinal ciliary grooves running in between protrusion. *(L)* Lip protrusion. *(R)* Longitudinal ribs covering peripheral microtubule doublets. Arrows point to fine fibrils (or folds). Arrowheads point to particles on the surface of the connecting cilium. Bar, 100 nm. × 260,000.

topographic fine structure by using thin coatings of low atomic number metals whose thickness approached the mean escape depth of SE (<2 nm). The signal collection was improved by shielding the objective pole piece with an aluminum plate coated with carbon for absorbing BSE. Thin, continuous, fine crystalline coatings of Nb or Cr obtained with a recently introduced Penning sputtering procedure eliminated the blanketing of topographic details by large metal crystals and reduced BSE generation. Under such conditions, high brightness electron sources, like LaB_6 or field emitter guns were necessary to generate sufficient beam current. However, high beam currents introduce severe beam damage on the specimen's surface which have so far limited high magnification work. Most of the electron beam energy converts into heat by inelastic scattering. Heat accumulates when thermal conductivity of the surface coating is reduced in films less than ~5 nm thick. To avoid this complication caused by thin films, we used low atomic number metals for coating and operated the microscope at high accelerating voltage, which reduced inelastic scattering and diminished beam damage at the specimen surface, relocating it into the depth of the specimen. High accelerating voltage is also necessary to reduce beam diameter, a precondition for high resolution. Extensive heat damages fragile surface structures (33), such as the filaments which span the grooves of the PRC (Fig. 3 *c*). These filaments were partially preserved by the preparation procedure used. They survived the impact of the electron probe during microscopy only when coated by Nb, but were completely lost when the specimens were decorated by Au (Figs. 2 *a* and *b* and 3 *a*). With the SE-I image mode, the level of resolution attained is comparable to the beam diameter (1 nm in our case); hence, visualization of surface detail becomes possible at the macromolecular level, e.g., the thin filaments or membrane folds seen on the CC surface (Fig. 5 *c*).

By using high resolution SE-I SEM, we have obtained a new, unique view of the organization of the junctional region of the inner and outer segments of frog retinal rod cells, and we have found and defined in detail a highly ordered new surface domain—the periciliary ridge complex—on the apical surface of the inner segment. The main components of the complex are an invagination from the bottom of which the ciliary shaft emerges, and a set of nine rigid ridges separated by grooves molded into the conical wall of the invagination which extend laterally on the apical surface of the inner segment. The complex has radial symmetry clearly related to the ninefold radial symmetry of the connecting cilium.

The periciliary ridge complex was not described in earlier TEM studies despite the fact that the emergence of the cilium from an invagination on the apical plasmalemma of the inner segment was repeatedly noted (7, 20). More recently, Andrews (1) described radiating parallel rows of intramembranous particles (IMP) and ridges in replicas of freeze-cleaved photoreceptor cells of fish, reptiles, and amphibia. He also noted "dimples" adjacent to the particle rows which resembled the exocytosis of synaptic vesicles at synaptic terminals observed by Heuser et al. (13). These rows of particles and ridges in Andrews' freeze-fracture study probably correspond to the ridges we have observed by SEM, but the ninefold symmetry around the cilium and the correlation of the ridges and grooves of the periciliary ridge complex to the invagination around the cilium were not revealed on the shallow surfaces selectively exposed by freeze-fracture. In our SEM study, looking on the surface of the ridges and grooves, additional fine structural details are revealed, i.e., filaments that bridge the grooves. The significance of these filamentous structures remains to be established by further work. They may represent true structures, remnants of the fibrillary material seen by TEM, or some other artifact. The existence of an invagination surrounding the base of the connecting cilium was also observed recently by video-enhanced, high resolution, differential interference light microscopy in retinal fragments freshly collected from living frog retinal rods (29), a finding which indicates that the deep invagination of the complex is not an artifact introduced by our preparation procedures. The periciliary ridge complex is topographically such an intricate structure that the TEM images of its profiles found in longitudinal, transverse, or oblique sections through the junctional region were never before associated with a realistic three-dimensional model. Once the three-dimensional organization of the complex was recognized by SEM, it was relatively easy to demonstrate complete correspondence of the two sets of images. The use of thin sections cut at appropriate angles (as done in this project) were particularly helpful in establishing this correlation. A diagram of our current understanding of the PRC is presented in Fig. 7.

It is already established—as a result of cell fractionation (23), autoradiographic (5, 46), freeze-fracture (4), and immunocytochemical experiments (25, 27, 30)—, that opsin is synthesized and inserted into membrane in the rough ER of the rod inner segment and that it passes through the Golgi complex before appearing in carrier vesicles clustered under the apical plasmalemma in the vicinity of the basal body of the connecting cilium. From the evidence presented in this article, we can conclude that these carrier vesicles are dissociated with the periciliary ridge complex. We hypothesize that they fuse on or near the grooves of the complex. Invaginations of the apical plasmalemma with a characteristically high population density of 10-nm intramembranous particles (seen in replicas of freeze-cleaved specimens) have been interpreted by Besharse and Pfenninger (4) as fused vesicular carriers; they may correspond at least in part to the grooves of the PRC.

Kinetic experiments have further established that, after the vesicle carrier stage, opsin appears in disks at the basal end of the outer segment (11, 44, 47). Biochemical, immunocytochemical, and freeze-fracture electron microscopic data indicate that opsin is present in these disks at a higher concentration than anywhere else in the cell (4, 22, 25).

At present, a major problem still in need of a solution concerns the pathways and means (forces) involved in the transport of newly synthesized opsin from the apical vesicular carriers of the IS to the proximal disks of the OS. The following premises and constraints must be considered in the discussion of a possible solution. The amount of opsin transported is unusually large: as much as 80 million molecules per day in the toad and 30 million in the frog (the equivalent of 10^6 opsin molecules per disk). The rate of transport shows diurnal variations: it is maximal in the morning (3). The transport is vectorial and seems to operate against an opsin concentration gradient (30).

As far as pathways are concerned, two alternatives may be considered. The first postulates transfer by direct fusion of the apical plasmalemma of the inner segment with the membrane of the most proximal disk of the outer segment (38); the other assumes that opsin moves along the membrane of the connecting cilium (30). The first postulate, which bypasses the connecting cilium, is unlikely given the low concentration of opsin in the apical membrane (Fig. 6 *a*), and the lack of reliable

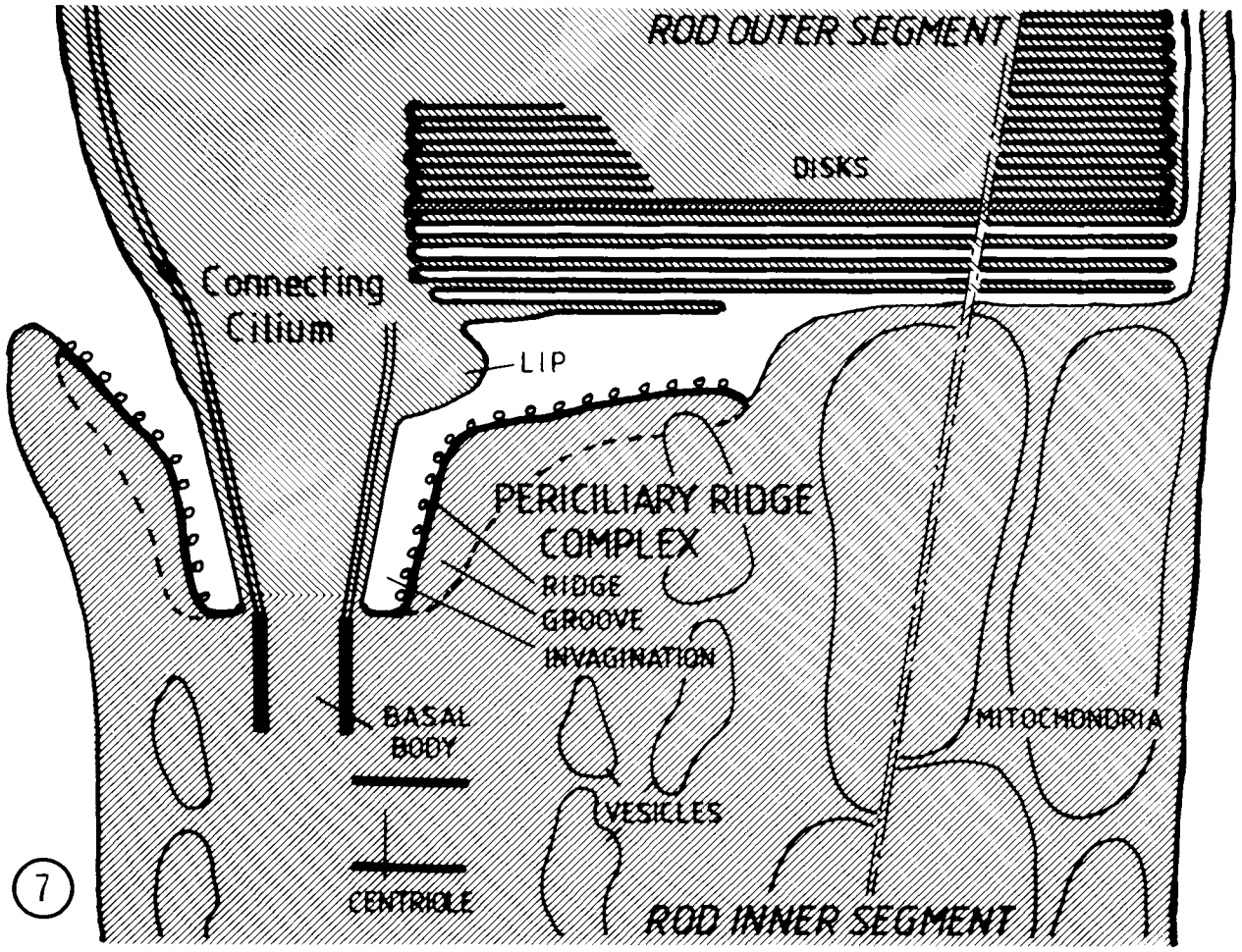

FIGURE 7 Diagram of the organization of a periciliary ridge complex and of its associated subcellular components in a rod cell of the frog retina. The diagram is restricted to the junctional region between the inner and outer segments of the retinal rod. The width of the cell is shortened as indicated by the gap (dashed lines) in the right half of the diagram.

morphological evidence of fusion between the membranes concerned. The second postulate takes into account the permanent membrane continuity along the connecting cilium and the high concentration of opsin vesicular carriers in the vicinity of the basal body. The periciliary ridge complex we have described appears to be located in the expected position for an opsin collector, and the remarkable correspondence of its radial symmetry with that of the connecting cilium suggests that the complex may impart directionality and spacial restrictions (in the sense of preferred lanes) to the opsin transport. At present the major difficulty in accepting this postulate stems from the fact that attempts to localize opsin in the plasmalemma of the basal portions of the connecting cilium have demonstrated only a low density of label (41). It is possible that the transport is restricted spacially: if it occurs, for instance, on a few lanes along the ciliary plasmalemma, it might be missed when examining thin sections by TEM-immunocytochemistry since the section is penetrated only to a small extent by antibodies (21). Freeze-fracture images of the CC plasma membrane of rat rods demonstrate circumferential rows of IMPs in the proximal CC (19, 39), and longitudinally oriented arrays of IMPs in the distal CC (19). Morphological evidence of disk morphogenesis at the upper portion of the CC supports the second postulate. We observe that disks expand above the eccentrically placed cilium until they reach full diameter of the ROS (Fig. 5*a*). These images directly confirm the model of disk morphogenesis of Steinberg et al. (43) which proposed that disks form by evagination from the CC plasmalemma. The liplike PM protrusions, rich in opsin (Fig. 6*a*), increased in size at times of disk assembly and were radially distributed on the CC circumference along with the CC longitudinal ribs (Fig. 5*b*). This may also indicate a functional specialization of the CC in disk formation. Additional experiments are in progress to evaluate if the lips change their shape during the light cycle.

Among the forces to be considered, lateral diffusion within the plasmalemma and active transport along a spacially restricted pathway are consistent with the organization of the cilium revealed in this study. Data on the lateral diffusion of rhodopsin in disk membranes in situ are available from the work of Poo and Cone (37) and Liebman and Entine (17), which have given a lateral diffusion coefficient as high as $5 \cdot 10^9$ $cm^2 \cdot s^{-1}$. At this rate, opsin molecules moving in a single row (at 2.5-nm intervals) along the cilium could deliver the opsin in 30 disks/d to the frog rod outer segment, provided that disk membranes act as a sink for opsin even in their forming stage when they are still in continuity with the plasmalemma. Lateral diffusion clearly requires a downhill gradient; hence an efficient sink in the OS would be necessary to eliminate a diffusion barrier of accumulated opsin. It also requires restrictions imposed to opsin diffusion from the PRC to the rest of the IS plasmalemma. If more than one row or lane is open for diffusion along the CC, the time required for

the transport of the daily amount of opsin could be considerably shorter. Although at present diffusion cannot be ruled out as a possible solution, certain limiting assumptions may eliminate it when properly checked. One assumption is that opsin lateral diffusion of opsin in the plasmalemma is comparable to that in disk membrane; however, lateral diffusion of proteins in the plasmalemma of other cells is considerably slower. Other molecules within the cilium may also alter diffusion rates. Finally, the actual time available for transport of most of the opsin molecules is still uncertain.

The other alternative is active transport in which mitochondria accumulated near the PRC, and molecules associated with the microtubular doublets are involved. Fibrillar connections between the doublets and the plasmalemma are regularly seen and an analogy with dynein arms can be invoked, although in this case active connections are postulated between microtubules and ciliary membranes rather than between microtubules. It is clear that this active transport solution implies substantial and unprecedented modifications of the dynein model or the use of a different motive protein.

The study was supported in part by U. S. Public Health Service research grants GM-21714, EY-3239, EY-845, and the Veterans Administration.

Received for publication 9 August 1982, and in revised form 4 October 1982.

REFERENCES

1. Andrews, L. 1982. Freeze-fracture studies of vertebrate photoreceptor membranes. *In* Structure of the Eye. J. G. Hollyfield, editor. Elsevier Biomedical, New York, Amsterdam, Oxford. 11–23.
2. Basinger, S., D. Bok, and M. O. Hall. 1976. Rhodopsin in the rod outer segment plasma membrane. *J. Cell Biol.* 69:29–42.
3. Besharse, J. C., J. G. Hollyfield, and M. E. Rayborn. 1977. Turnover of rod photoreceptor outer segments. I. Membrane addition and loss in relationship to temperature. *J. Cell Biol.* 75:490–506.
4. Besharse, J. C., and K. H. Pfenninger. 1980. Membrane assembly in retinal photoreceptors. I. Freeze-fracture analysis of cytoplasmic vesicles in relationship to disc assembly. *J. Cell Biol.* 87:451–463.
5. Bok, D., M. O. Hall, and P. O'Brien. 1977. The biosynthesis of rhodopsin as studied by membrane renewal in rod outer segments. *In* International Cell Biology 1976–1977. B. R. Brinkley and K. R. Porter, editors. The Rockefeller University Press, New York. 608–617.
6. Boyde, A., and S. Boyde. 1980. Further studies of specimen volume changes during processing for SEM: including some plant tissue. *Scanning Electron Microsc.* 117(II):124–132.
7. Cohen, A. I. 1960. The ultrastructure of the rods in the mouse retina. *Am. J. Anat.* 107:23–48.
8. Crewe, A. W., and P. S. D. Linn. 1976. The use of backscattered electrons for imaging purposes in a scanning electron microscope. *Ultramicroscopy.* 1:231–238.
9. R. U. C. Dawson, D. C. Elliott, W. H. Elliott, and K. M. Jones, editors. Dawson, R. U. C. 1969. Physiological media. *In* Data for Biochemical Research. Oxford University Press. 508.
10. Goldman, B. M., and G. Blobel. 1981. In vitro biosynthesis, core-glycosylation, and membrane integration of opsin. *J. Cell Biol.* 90:236–242.
11. Hall, M. O., D. Bok, and A. D. E. Bacharach. 1969. Biosynthesis and assembly of the rod outer segment membrane system. Formation and fate of visual pigment in the frog retina. *J. Mol. Biol.* 45:397–406.
12. Hollyfield, J. G., J. C. Besharse, and M. E. Rayborn. 1977. Photoreceptor outer segments: accelerated membrane renewal in rods after exposure to light. *Science (Wash. D. C.).* 196:533–536.
13. Heuser, J. E., T. S. Reese, M. J. Dennis, Y. Jan, L. Jan, and L. Evans. 1979. Synaptic vesicle exocytosis captured by quick freezing and correlated with quantal transmitter release. *J. Cell Biol.* 81:275–300.
14. Jacopić, E., A. Brunegger, R. Essl, and G. Windisch. 1978. A sputter source for electron microscopic preparation. *Electron Microsc. 1978,* I; Microscop. Society of Canada, Toronto, Ontario, M5S 1A1:150–151.
15. Kinney, M. S., and S. K. Fischer. 1978. The photoreceptors and pigment epithelium of the adult *Xenopus* retina: morphogenesis and outer segment renewal. *Proc. R. Soc. Lond. Ser. Biol. Sci.* 201:149–167.
16. Kraehenbuhl, J. P., and J. D. Jamieson. 1974. Localization of intracellular antigens by immunoelectron microscopy. *Int. Rev. Exp. Pathol.* 13:1–53.
17. Liebman, P. A., and G. Entine. 1974. Lateral diffusion of visual pigment in photoreceptor disk membranes. *Science (Wash. D. C.).* 185:457–459.
18. McLean, J. D., and S. J. Singer. 1970. A general method for the specific staining of intracellular antigens with ferritin-antibody conjugates. *Proc. Natl. Acad. Sci. U. S. A.* 65:122–128.
19. Matsusaka, T. 1974. Membrane particles of the connecting cilium. *J. Ultrastruct. Res.* 48:305–312.
20. Nilsson, S. E. G. 1964. Receptor cell outer segment development and ultrastructure of the disk membranes in the retina of the tadpole (*Rana pipiens*). *J. Ultrastruct. Res.* 11:581–620.
21. Nir, I., B. G. Schneider, and D. S. Papermaster. 1982. Quantitative analysis of immunocytochemical labeling density of antiopsin on rod outer segments. *Invest. Ophthalmol. Visual Sci.* 1(Suppl.):22, 283.
22. Papermaster, D. S., and W. J. Dreyer. 1974. Rhodopsin content in the outer segment membranes of bovine and from retinal rods. *Biochemistry.* 13:2438–2444.
23. Papermaster, D. S., C. A. Converse, and J. Siu. 1975. Membrane biosynthesis in the frog retina: opsin transport in the photoreceptor cell. *Biochemistry.* 14:2438–2442.
24. Papermaster, D. S., C. A. Converse, and M. Zorn. 1976. Biosynthetic and immunochemical characterization of a large protein in frog and cattle rod outer segment membranes. *Exp. Eye Res.* 23:105–115.
25. Papermaster, D. S., B. G. Schneider, M. A. Zorn, and J. P. Kraehenbuhl. 1978. Immunocytochemical localization of opsin in the outer segments and Golgi zones of frog photoreceptor cells. *J. Cell Biol.* 77:196–210.
26. Papermaster, D. S., B. G. Schneider, M. A. Zorn, and J. P. Kraehenbuhl. 1978. Immunocytochemical localization of a large intrinsic membrane protein to the incisures and margins of frog rod outer segment disks. *J. Cell Biol.* 78:415–425.
27. Papermaster, D. S., B. G. Schneider, and J. C. Besharse. 1979. Assembly of rod photoreceptor membranes: immunocytochemical and autoradiographic localization of opsin in smooth vesicles of the inner segment. *J. Cell Biol.* 83(2, Pt. 2):275*a*. (Abstr.)
28. Papermaster, D. S., Y. Burstein, and I. Schechter. 1980. Opsin mRNA isolation from bovine retina and partial sequence of the *in vitro* translation product. *Ann. N. Y. Acad. Sci.* 343:347–355.
29. Papermaster, D. S., and R. D. Allen. 1981. Clustered vesicles in the juxtaciliary cytoplasm of rod inner segments revealed in living cells by high resolution Allen video-enhanced-differential interference contrast microscopy. *Invest. Ophthalmol. Visual Sci.* 1(Suppl.):20, 152.
30. Papermaster, D. S., and B. G. Schneider. 1982. Biosynthesis and morphogenesis of outer segment membranes in vertebrate photoreceptor cells. *In* Cell Biology of the Eye. D. McDevitt, editor. Academic Press, NY. 475–531.
31. Papermaster, D. S., P. M. Reilly, and B. G. Schneider. 1982. Cone lamellae and red and green rod outer segment disks contain a large intrinsic membrane protein on their margins: an ultrastructural immunocytochemical study of frog retinas. *Vision Res.* In press.
32. Peters, K.-R. 1980a. Improved handling of structural fragile cell-biological specimens during electron microscopic preparation by the exchange method. *J. Microsc.* 118:429–441.
33. Peters, K.-R. 1980b. Penning sputtering of ultrathin metal films for high resolution electron microscopy. *Scanning Electron Microsc.* 1(1980):143–154.
34. Peters, K.-R. 1982a. Generation, collection and properties of an SE-I enriched signal suitable for high resolution SEM on bulk specimens. *Proceedings Conference on Electron Beam Interaction.* SEM Inc., Chicago. In press.
35. Peters, K.-R. 1982b. Validation of George and Robinson SE-I signal theorem. Implication for ultrahigh resolution SEM on bulk untilted specimens. *In* 40th Annual Proceedings of the Electron Microscopy Society of America. G. W. Bailey, editor. Claitors Publishing Div., Baton Rouge, LA. 368–369.
36. Peters, K.-R., B. G. Schneider, and D. S. Papermaster. 1981. Ultrahigh resolution scanning electron microscopy of a periciliary ridge complex of frog retinal rod cells. *J. Cell Biol.* 91(2, Pt. 2):273*a*. (Abstr.)
37. Poo, M. M., and R. A. Cone. 1974. Lateral diffusion of rhodopsin in the photoreceptor membrane. *Nature (Lond.).* 247:438–441.
38. Richardson, T. M. 1969. Cytoplasmic and ciliary connections between the inner and outer segments of mammalian visual receptors. *Vision Res.* 9:727–731.
39. Röhlich, P. 1975. The sensory cilium of retinal rods is analogous to the transitional zone of motile cilia. *Cell Tissue Res.* 161:421–430.
40. Schechter, I., Y. Burstein, R. Zemell, E. Ziv, F. Kantor, and D. S. Papermaster. 1979. Messenger RNA of opsin from bovine retina: isolation and partial sequence of the *in vitro* translation product. *Proc. Natl. Acad. Sci. U. S. A.* 76:2654–2658.
41. Schneider, B. G., and D. S. Papermaster. 1981. Immunocytochemical localization of opsin in the connecting cilium of rat and *Xenopus* rods. *Invest. Ophthalmol. Visual Sci.* 1(Suppl.):20–76.
42. Seiler, H. 1967. Some current problems in SE emission. *Z. Angew. Physik.* 22:249–263.
43. Steinberg, R. H., S. K. Fisher, and D. H. Anderson. 1980. Disc morphogenesis in vertebrate photoreceptors. *J. Comp. Neurol.* 190:501–518.
44. Young, R. W. 1967. The renewal of photoreceptor cell outer segments. *J. Cell Biol.* 33:61–72.
45. Young, R. W. 1968. Passage of newly formed protein through the connecting cilium of retinal rods in the frog. *J. Ultrastruct. Res.* 23:462–473.
46. Young, R. W. 1976. Visual cells and the concept of renewal. *Invest. Ophthalmol.* 15:700–725.
47. Young, R. W., and B. Droz. 1968. The renewal of protein in retinal rods and cones. *J. Cell Biol.* 39:169–184.